



**HAL**  
open science

## **Paleomagnetic of Upper Jurassic to Lower Cretaceous volcanic and sedimentary rocks from the western Tarim and implications for inclination shallowing and absolute dating of the M0 (ISEA) chron.**

Stuart A. Gilder, Yan Chen, Jean-Pascal Cogné, Xiaodong Tan, Vincent Courtillot, Dongjiang Sun, Yongan Li

### **► To cite this version:**

Stuart A. Gilder, Yan Chen, Jean-Pascal Cogné, Xiaodong Tan, Vincent Courtillot, et al.. Paleomagnetic of Upper Jurassic to Lower Cretaceous volcanic and sedimentary rocks from the western Tarim and implications for inclination shallowing and absolute dating of the M0 (ISEA) chron.. *Earth and Planetary Science Letters*, 2003, 206, pp.587-600. 10.1016/S0012-821X(02)01074-9 . hal-00069402

**HAL Id: hal-00069402**

**<https://insu.hal.science/hal-00069402>**

Submitted on 20 Sep 2006

**HAL** is a multi-disciplinary open access archive for the deposit and dissemination of scientific research documents, whether they are published or not. The documents may come from teaching and research institutions in France or abroad, or from public or private research centers.

L'archive ouverte pluridisciplinaire **HAL**, est destinée au dépôt et à la diffusion de documents scientifiques de niveau recherche, publiés ou non, émanant des établissements d'enseignement et de recherche français ou étrangers, des laboratoires publics ou privés.

# **Paleomagnetism of Upper Jurassic to Lower Cretaceous volcanic and sedimentary rocks from the western Tarim Basin and implications for inclination shallowing and absolute dating of the M-0 (ISEA?) chron**

**Stuart Gilder<sup>a</sup>, Yan Chen<sup>b</sup>, Jean-Pascal Cogné<sup>a</sup>, Xiaodong Tan<sup>a</sup>, Vincent Courtillot<sup>a</sup>, Dongjiang Sun<sup>c</sup> and Yongan Li<sup>c</sup>**

<sup>a</sup> Institut de Physique du Globe de Paris, Laboratoire de Paléomagnétisme, 4 place Jussieu, 75252, Paris Cedex 05, France

<sup>b</sup> Département des Sciences de la Terre, Université d'Orléans, P.O. Box 6759, 45067, Orléans Cedex 02, France

<sup>c</sup> Institute of Geology and Mineral Resources, Bureau of Geology and Mineral Resources of Xinjiang Uygur Autonomous Region, 16 Youhao Beilu, Urumqi, PR China

## **Abstract**

Stepwise demagnetization isolates a stable magnetic component in 13 sites of basalt flows and baked sediments dated at  $113.3 \pm 1.6$  Ma from the Tuoyun section, western Xinjiang Province, China. Except for one flow from the base of the  $\sim 300$  m thick section, the rest have exclusively reversed polarity. The sequence correlates with chron M-0 in some geomagnetic polarity time scales, which potentially places the section just before the start of the Cretaceous Long Normal polarity superchron. Five of 11 sites of Early Cretaceous red beds that underlie the basalts possess coherent directions that pass both fold and reversals tests. Six sites of Upper Jurassic red beds have a magnetic component that was likely acquired after folding in the Tertiary. The mean paleolatitude of the Lower Cretaceous red beds is  $11^\circ$  lower than that of the Lower Cretaceous basalts suggesting the red beds underestimate the true field inclination. We further test this result by calculating the paleolatitudes to a common point of the available Early Cretaceous to Present paleomagnetic poles from red beds and volcanic rocks from central Asian localities north of the Tibetan Plateau. We find that paleolatitudes of volcanic rocks roughly equal the paleolatitudes calculated from the reference Eurasian apparent polar wander path (APWP) and that paleolatitudes of red beds are generally  $10\text{--}20^\circ$  lower than the paleolatitudes of volcanic rocks and those predicted from the reference curve. Our study suggests that central Asian red beds poorly record the Earth's field inclination, which leads to lower than expected paleolatitudes. Good agreement in paleolatitudes from volcanic rocks and the Eurasian APWP argues against proposed canted and non-dipole field models.

**Author Keywords:** paleomagnetism; Asia; inclination shallowing; magnetostratigraphy; magnetic field; magnetic recording; basalt; red beds; Cretaceous; Jurassic

# 1. Introduction

The exceptional topographic relief and high strain rates in central Asia provide an excellent opportunity to quantify geologic effects of intracontinental deformation related to the India–Asia collision (Fig. 1). As paleomagnetism provides a means to constrain shortening amounts, this technique has been widely applied in the region. Early paleomagnetic studies concentrated on Cretaceous rocks, which produced a coherent picture of systematically increasing paleolatitudes and diminished shortening from south to north. The Cretaceous data suggested some 2700 km of total shortening occurred between India and Asia, of which  $1700\pm 600$  km was absorbed within Asia, with more than 1000 km of shortening taken up between the Tarim Basin and Siberia, north of the Tibetan plateau [1].

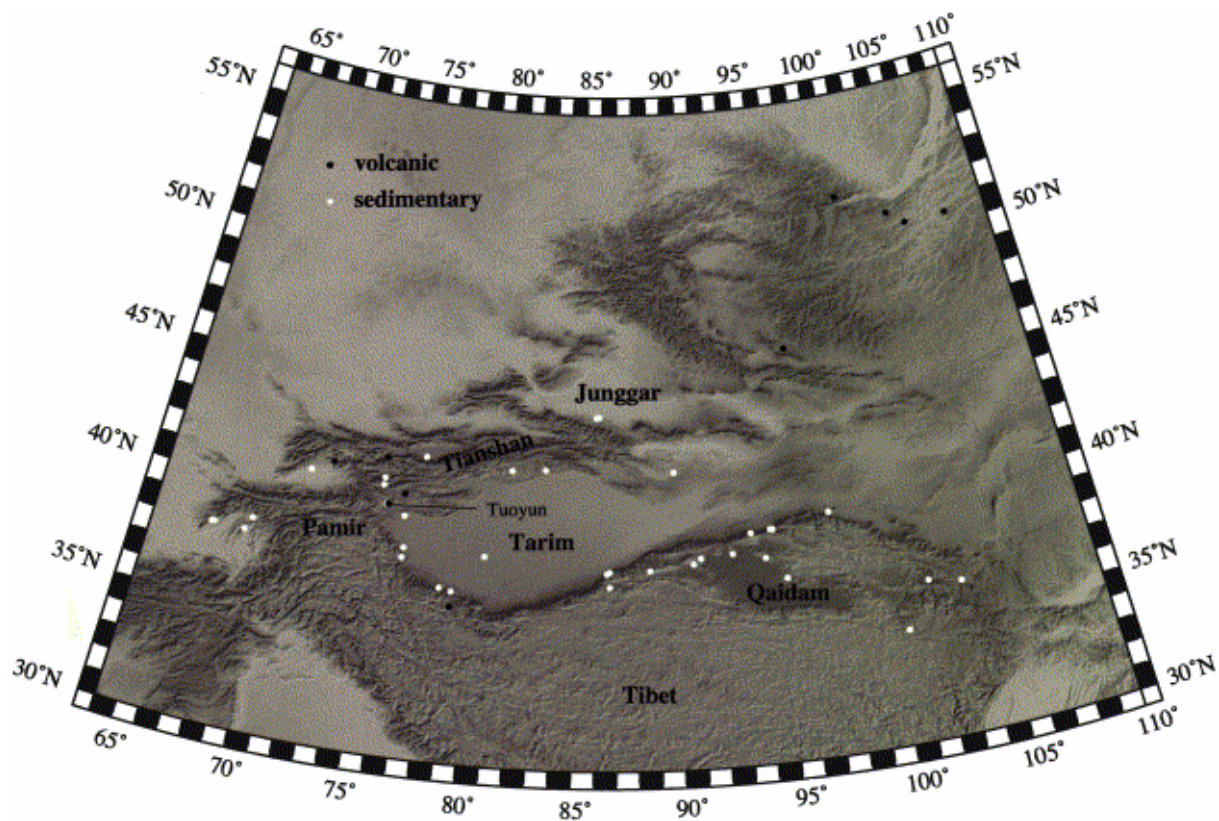


Fig. 1. Topographic map of central Asia showing distribution of volcanic and red bed localities used to construct Fig. 7.

When Cenozoic paleomagnetic results became available, however, the picture grew more complicated. Although the Cretaceous and Cenozoic paleolatitudes were virtually the same, the Eurasian apparent polar wander path (APWP), with which the poles from central Asia were compared, required about twice the amount of shortening for the Cenozoic data as for the Cretaceous data. Such quantities were incompatible with geologic observations and topographic constraints. Several hypotheses were proposed to explain this discrepancy such as poor age control, syn-sedimentary or compaction-induced inclination shallowing, tilted axial dipole, non-dipolar geomagnetic field geometry, tectonic shortening, tectonic escape, remagnetization, a poorly constrained APWP for Eurasia, and non-rigidity of the Eurasian plate [2, 3, 4, 5, 6, 7, 8, 9 and 10].

Two magnetostratigraphic studies have recently placed tight constraints on the ages of Upper Tertiary rocks and leave little doubt that tectonic shortening cannot explain the observed inclinations, which are some 15° shallower than at present [8 and 11]. The paleolatitudes of these Neogene data would require central Asia to have moved nearly 1000 km farther north than India in the past 20 Ma, a notion incompatible with all geologic observations. Gilder et al. [8] found that, among 25 studies carried out on Upper Jurassic to Neogene red beds in central Asia ( Fig. 1), the paleolatitudes were the same regardless of age. Syn-sedimentary inclination shallowing, which produces lower than expected paleolatitudes, was identified as the most probable cause. However, it is strange that the expected paleolatitudes change with time yet the observed paleolatitudes remain constant. This leads one to question, for example, if inclination shallowing has affected the Cenozoic rocks more than the Cretaceous ones, or if the Eurasian reference APWP is valid.

One way to test whether the paleolatitudes measured in red beds are real or artificial is to compare them with paleolatitudes derived from volcanic rocks, which are largely immune from shallowing effects. A drawback of volcanics, however, is that enough flows must be sampled in order to average out geomagnetic secular variation to yield a time-averaged pole, equivalent to the geocentric axial dipole field direction acting when the flows were emplaced. Often only a few flows are available for sampling and it is not clear whether secular variation has been sufficiently averaged. For example, Otofuchi et al. [12] sampled two Pleistocene basalt flows and found inclinations near the expected inclination from the reference APWP; whereas Thomas et al. [2] found much shallower than expected inclinations from two sites from a single ~50 Ma basalt flow and two sites of sediments baked by that flow. Recently, Bazhenov and Mikolaichuk [13] reported 18 sites drilled in a minimum of five Paleogene flows. The mean direction shows no shallowing with respect to the synthetic Siberian APWP. To better understand the origin of the shallow inclinations in central Asia, we undertook a paleomagnetic study of a ~300 m thick pile of basalt flows, of which we sampled a minimum of 11 flows in the Tuoyun section in western Xinjiang Province, China ( Fig. 1). Moreover, we sampled red beds that underlie, and are intercalated with, the basalts in order to compare the directions of the two rock types. Paleomagnetic data from the Tuoyun basalts were previously reported by Li et al. [14] and Meng et al. [15] and are discussed in light of our new findings.

## 2. Geologic setting, sampling and methods

Tuoyun village lies near the border of Kyrgyzstan at the westernmost limit of the Tarim Basin, in the southeastern Tianshan Mountains (Fig. 1). The section we sampled concerns a ~300 m thick pile of olivine-bearing basalts that are intercalated with sediments, as well as red beds of the Lower Cretaceous Kezilesu Group and the Upper Jurassic Kuzigongsu Formation that underlie the basalts [16] ( Fig. 2). The sediments were dated by regional correlation and we know of no direct fossil control. Geochemistry and  $^{40}\text{Ar}/^{39}\text{Ar}$  dating of the basalts are described in Sobel and Arnaud [17] who reported weighted mean  $^{40}\text{Ar}/^{39}\text{Ar}$  dates for whole rock and a plagioclase fraction from one flow (sample 91T111) as  $113.3 \pm 1.6$  (1 $\sigma$ ) and  $119.7 \pm 8.1$  Ma, respectively. Biotite extracted from gabbro and from diabase sills that intrude the series yielded weighted mean ages ranging from 46 to 67 Ma.

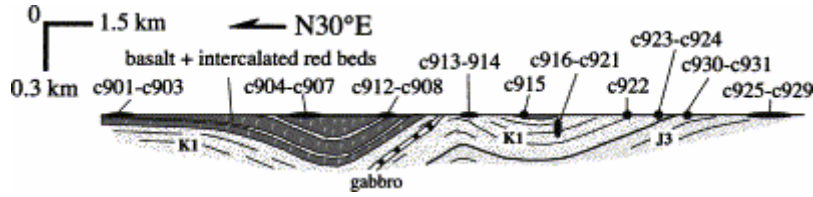


Fig. 2. Simplified cross-section of the Tuoyun section from field notes. K1 is Early Cretaceous and J3 is Upper Jurassic. Depth projection of gabbro dike is hypothetical.

A simplified structural profile of the Tuoyun section is shown in Fig. 2. Altogether we sampled 11 basalt sites, two sites of sediments (c909 and c911) intercalated in the basalt flows, 11 Lower Cretaceous red bed sites and seven Upper Jurassic red bed sites (Table 1). Each basalt site represents at least one discrete flow. Paleomagnetic samples were collected with a gasoline-powered drill and oriented with magnetic and sun compasses, the latter to check and correct for local declination anomalies, which averaged  $3.4 \pm 2.2^\circ$  ( $1\sigma$ ). Samples cut from each core underwent stepwise (averaging 15 steps) thermal or alternating field (AF) demagnetization. Magnetic remanences were measured with a 2G, three-axis DC SQUID magnetometer (red beds) or an AGICO JR-5 spinner magnetometer (basalts) housed in a magnetically shielded room at the Institut de Physique du Globe de Paris. Magnetic components were determined using principal component analysis [18], and directions were analyzed using Fisher [19] statistics and the Watson and Enkin [20] fold test applying 1000 simulations and assuming a  $5^\circ$  uncertainty on bedding corrections. Data were treated using software developed by Cogné [21] and R. Enkin (unpublished).

Table 1. Paleomagnetic data from the Tuoyun section, western Xinjiang Province

Site	Lith.	Age	Slon	Slat	n/N	D <sub>g</sub>	I <sub>g</sub>	D <sub>s</sub>	I <sub>s</sub>	k	$\alpha_{95}$	Strike	Dip	Plat	Plon
c901	bas	K1	75°20'02.4"	40°17'38.8"	66	172.6	-43.9	22.48	-70.2	60.1	8.7	55.0	39.0	-57.2	304.9
c902	bas	K1	75°20'02.4"	40°17'38.8"	66	170.6	-33.5	22.08	-73.8	18.5	16.0	62.0	47.0	-59.1	293.7
c903	bas	K1	75°20'02.4"	40°17'38.8"	77	155.4	-10.5	16.12	-55.9	2158	4.1	57.7	46.0	-74.8	156.5
c904	bas	K1	75°19'25.6"	40°15'53.5"	66	204.3	-4.1	21.28	-38.0	46.3	10.0	86.1	39.6	-56.4	9.7
c905	bas	K1	75°19'25.6"	40°15'53.5"	66	188.9	-9.7	19.51	-47.9	321.6	3.7	86.1	39.6	-73.3	23.2
c906	bas	K1	75°19'25.6"	40°15'53.5"	66	214.1	-8.3	22.62	-37.5	289.4	3.9	86.1	39.6	-46.4	357.4
c907	bas	K1	75°19'25.6"	40°15'53.5"	12/12	229.7	0.3	23.63	-22.0	35.9	5.9	86.1	39.6	-52.9	339.2
c908	bas	K1	75°18'58.2"	40°14'52.2"	66	157.0	-57.0	19.09	-37.0	157.6	5.4	322.2	35.5	-68.3	46.6
c909	red-b	K1	75°18'58.2"	40°14'52.2"	88	235.7	-76.9	23.64	-37.9	104.4	5.4	326.7	39.0		
c910	bas	K1	75°18'58.2"	40°14'52.2"	66	101.4	-74.7	21.48	-60.2	105.4	6.6	326.7	39.0	-63.8	331.9
c911	red-b	K1	75°18'58.2"	40°14'52.2"	99	166.2	-73.3	20.86	-43.4	103.4	5.1	319.3	37.0		
c912	bas	K1	75°18'58.2"	40°14'52.2"	46	109.4	-68.0	19.08	-58.5	42.6	14.2	319.3	37.0	-81.7	348.6
c913	red	K1	75°18'30.7"	40°14'14.4"	07							95.0	32.0		
c914	red	K1	75°18'30.7"	40°14'14.4"	01/2							92.0	40.0		
c915	bas	K1	75°18'32.3"	40°13'45.2"	77	38.6	35.1	38.7	43.8	173.6	4.6	128.1	8.7	54.7	177.7
c916	red	K1	75°19'16.6"	40°12'51.4"	08							215.0	21.0		
c917	red	K1	75°19'16.6"	40°12'51.4"	3/6	59.5	32.4	41.5	48.6	133.2	10.7	193.1	26.0	54.7	169.6
c918	red	K1	75°19'26.9"	40°12'47.2"	04							186.0	24.0		
c919	red	K1	75°19'26.9"	40°12'47.2"	07							199.0	29.0		
c920	red	K1	75°19'26.9"	40°12'47.2"	69	222.1	-11.4	21.61	-33.2	22.2	14.5	162.4	26.0	-51.9	10.0
c921	red	K1	75°19'26.9"	40°12'47.2"	89	225.4	-18.6	21.76	-36.8	26.7	10.9	169.6	23.5	-52.5	5.6
c922	red	K1	75°19'27.4"	40°11'54.2"	68	290.1	-42.5	22.37	-35.0	32.5	11.9	240.6	32.5	47.2	181.4
c923	red	K1	75°19'02.6"	40°11'34.2"	5/6	58.1	66.0	30.8	38.9	65.9	10.2	276.6	33.0	58.2	191.0
c924	red	K1	75°19'02.6"	40°11'34.2"	08							272.0	33.0		
c925	red	J3	75°18'42.3"	40°10'49.6"	7/10	30.5	63.1	10.2	48.2	43.5	9.3	247.2	20.0	76.3	214.9
c926	red	J3	75°18'42.3"	40°10'49.6"	4/8	12.0	65.4	0.7	49.1	52.8	12.8	252.3	17.7	79.8	251.9
d27	red	J3	75°18'42.3"	40°10'49.6"	6/8	35.0	63.0	1.32	48.9	84.8	7.3	247.8	20.0	75.0	205.1
d28	red	J3	75°18'42.0"	40°10'30.8"	9/9	18.3	54.6	1.5	44.9	31.8	9.3	223.9	17.0	76.2	249.8
d29	red	J3	75°18'42.0"	40°10'30.8"	8/8	40.2	64.9	9.4	59.1	127.1	4.9	224.0	17.0	82.8	165.2
d30	red	J3	75°19'00.8"	40°11'05.4"	9/9							251.0	24.0		
d31	red	J3	75°19'00.6"	40°11'05.5"	8/8	33.5	69.2	10.4	58.1	41.9	8.7	245.9	15.7	81.9	172.3
Mean K1 basalts					11/11	7.5	35.8			4.5	24.1				
Mean K1 basalts					11/11			29.4	51.4	15.3	12.1		13.6	66.6	170.7
Mean K1 basalts+red beds-b					13/13	8.0	43.1			4.5	22.0				
Mean K1 basalts+red beds-b					13/			31.9	49.9	16.3	10.6		12.0	64.1	172.1
Mean K1 red beds					13										
Mean K1 red beds					5/11	53.6	34.5			12.1	22.9				
Mean K1 red beds					8/			37.9	38.6	127.4	6.8		6.1	53.2	183.4
Mean J3 red beds					11										
Mean J3 red beds					6/7	27.7	63.7			140.9	5.7		7.9	68.9	141.0
Mean J3 red beds					6/7			7.3	51.5	148.1	5.5				

Abbreviations: Lith., lithology; bas, basalt; red, red bed; red-b, baked red bed; Slat (Plat), latitude of site (pole); Slon (Plon), longitude of site (pole); n/N, number of samples used to calculate mean direction/number of samples demagnetized; D, declination; I, inclination; g, in situ (geographic) coordinates; s, tilt-corrected (stratigraphic) coordinates (at 100% unfolding);  $\alpha_{95}$  ( $A_{95}$ ), the radius that the mean direction (pole) lies within 95% confidence; k, the best estimate of the precision parameter.

### 3. Results

Thermal and AF demagnetization isolated a single dominant magnetic component in all basalt samples after removing a recent field or weak viscous magnetization (Fig. 3). In most cases, complete demagnetization occurred in peak fields from 60 to 140 mT or between 540 and 580°C, suggesting that titanomagnetite is the dominant carrier of the magnetic remanence. Some samples, especially from sites c905 and c912, were fairly resistant to AF demagnetization and had about 40% of their initial intensities unblocking from 580 to 680°C, indicating the presence of hematite. Thermoremanent magnetization experiments using an AGICO CS-2 Kappabridge show a steep drop off in the 550–580°C range with a weak signal persisting thereafter that decreases with increasing temperature. Hysteresis parameters of 25 samples plot within the pseudo-single domain region on a Day diagram [22]; however, the grain sizes are probably pulled away from the single domain field toward the multidomain field due to the influence of hematite.

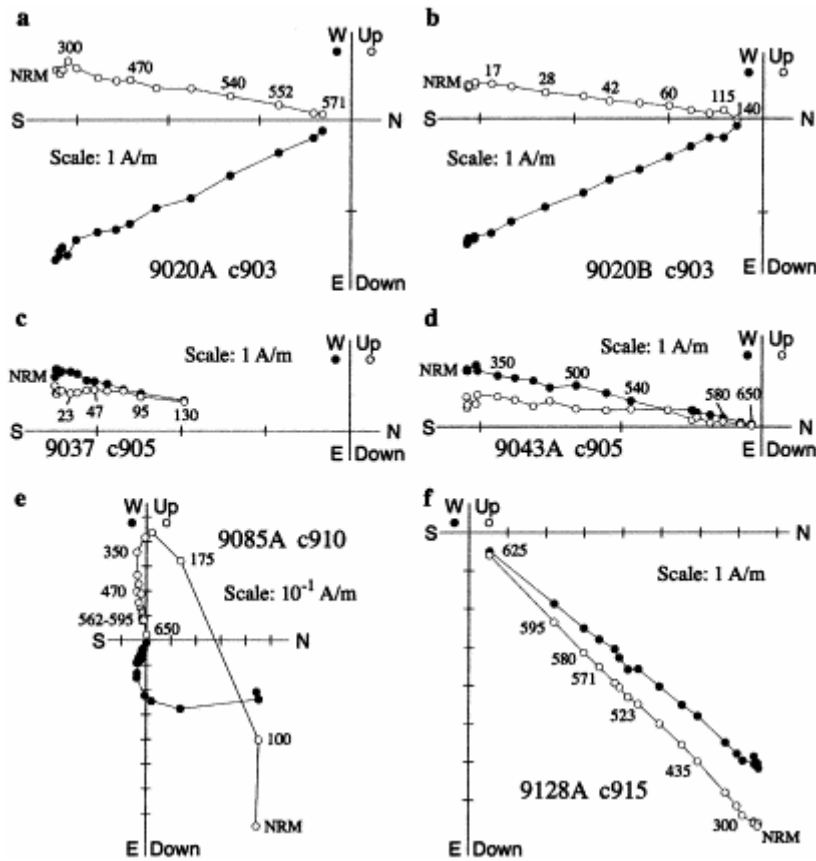


Fig. 3. Orthogonal demagnetization diagrams of basaltic rocks (sample number and corresponding sites listed) in in situ coordinates. Demagnetization steps in °C in all plots except b and c which are in mT. NRM is the natural remanent magnetization.

Remanent magnetization characteristics of the sediments varied widely. Average initial magnetic intensities of sites c909 and c911 were about 100 times greater than the other Lower Cretaceous red bed sites ( $7 \times 10^{-2}$  A/m vs.  $9 \times 10^{-4}$  A/m) and more than 10 times greater than the Upper Jurassic sites ( $5 \times 10^{-3}$  A/m). The former two sites exhibited linear demagnetization trajectories that decayed toward the origin in a narrow range of unblocking temperatures (Fig.

4a,b). Their strong intensities and demagnetization behaviors are consistent with the idea that they were baked above hematite Curie temperatures, i.e., that their magnetic remanences are thermal and not depositional or chemical in origin. We did not sample the basalt flows that immediately overlie sites c909 and c911. Sites c910 and c912, which overlie sites c909 and c911 by 23 m and 4 m, respectively, possess significantly different mean directions (Table 1). From our field observations and the demagnetization characteristics, we conclude that the mean directions of sites c901–c912 and c915 each represent an independent spot reading of the field.

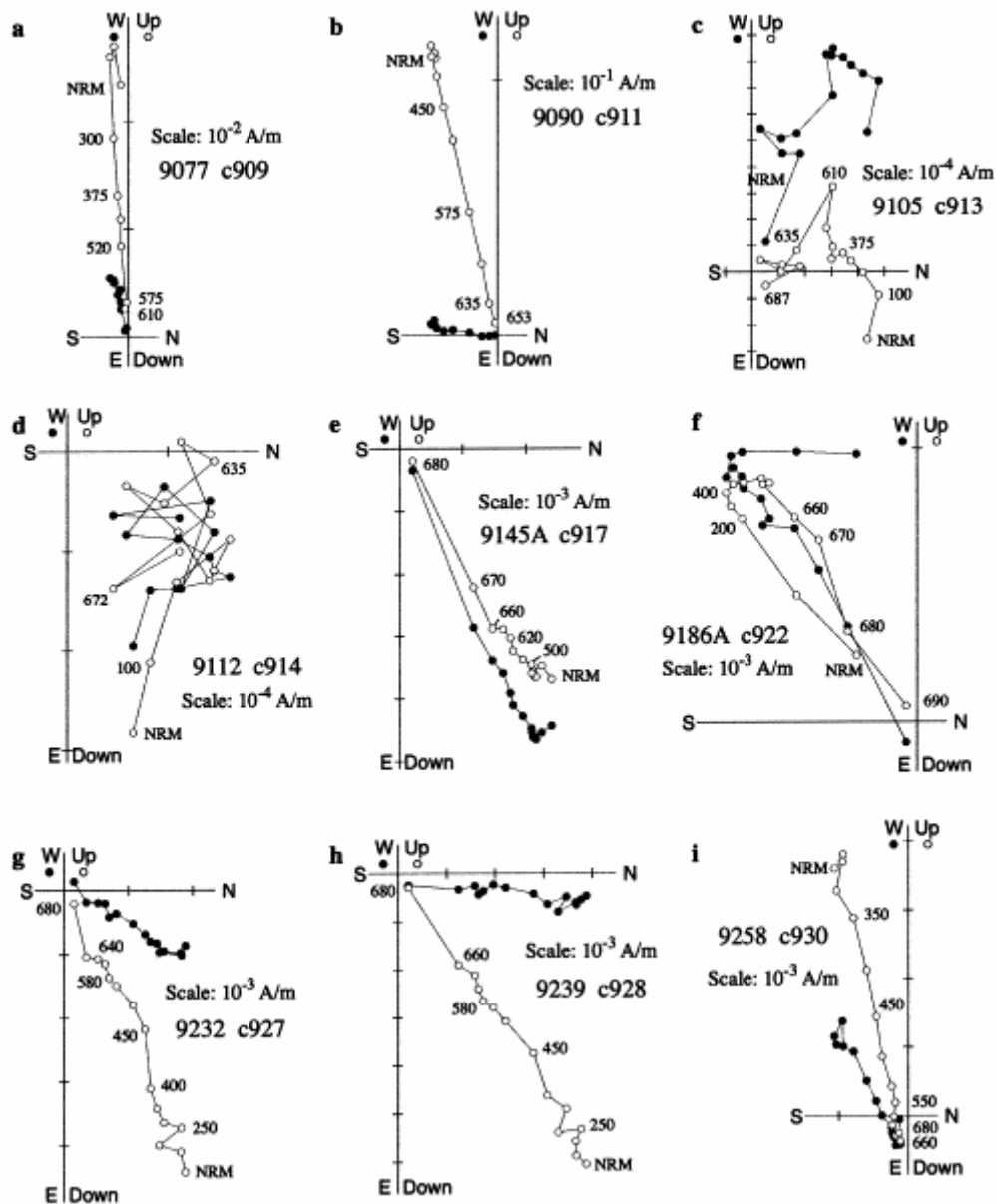


Fig. 4. Orthogonal demagnetization diagrams of sedimentary rocks (sample number and corresponding sites listed) in in situ coordinates. Demagnetization steps in °C in all plots. NRM is the natural remanent magnetization. Panels a and b from baked sediments, c–f from Lower Cretaceous red beds and g–i from Upper Jurassic red beds.

The other Lower Cretaceous red bed samples displayed quite variable demagnetization characteristics ranging from erratic or multiple component behavior (Fig. 4c,d) to a single,

stable component at high temperatures ( Fig. 4e,f). In general, sample directions from five sites exhibited a coherent, stable component pointing NNE and down or SSW and up in tilt-corrected coordinates, with roughly equal proportions of normal and reverse polarities. The other samples had unstable or quite scattered directions on the intra-site level. Samples from the Upper Jurassic red beds were dominated by a single magnetic component of normal polarity in all sites except one (c930) ( Fig. 4g–i). However, individual directions from this latter site, although well defined, were so dispersed that it was omitted from further consideration.

When applying the fold test we separated the sites into three groups: (1) all basalt sites plus baked sedimentary sites c909 and c911, (2) Lower Cretaceous red bed sites and (3) Upper Jurassic red bed sites (Table 1 and Fig. 5). For the first group, the test statistic maximized at  $102\pm 8\%$  unfolding which clearly demonstrates a pre-folding remanence (Fig. 5a). We regard it as a primary magnetization. The mean tilt-corrected direction is similar to those reported by Li et al. ([14] –  $D=19.6^\circ$ ,  $I=52.5^\circ$ ,  $N=11$ ,  $k=17$ ,  $\alpha_{95}=11.4^\circ$ ) and Meng et al. ([15] –  $D=12.7^\circ$ ,  $I=44.8^\circ$ ,  $N=10$ ,  $k=14.9$ ,  $\alpha_{95}=13.0^\circ$ ). The test statistic based on five of 11 sites of the Lower Cretaceous red beds maximizes at  $98\pm 19\%$  unfolding (Fig. 5b). The positive fold test and dual polarities suggest the remanence is primary. The bedding attitudes of the Upper Jurassic red beds do not allow the fold test to be applied with any significance although the test statistic maximizes at 27% unfolding ( Fig. 5c). If uncertainty on bedding attitude measurements is increased from  $5^\circ$  to  $8^\circ$  then the fold test excludes the case at 100% unfolding with a maximum at  $14\pm 56\%$ . It is strange that the stable magnetization component is only represented by normal polarity, yet the reversal frequency was relatively high during that time interval [23]. If the remanence was primary, one would have to explain why the Cretaceous basalts and red beds were rotated respectively  $19.0\pm 12.0^\circ$  and  $24.5\pm 5.8^\circ$  clockwise, yet the Upper Jurassic red beds were rotated  $-12.2\pm 8.9^\circ$  counterclockwise compared to coeval poles from the synthetic Eurasian APWP [24]. This would imply an about  $-34^\circ$  counterclockwise rotation of the Upper Jurassic strata before deposition of the Lower Cretaceous strata followed by a  $\sim 22^\circ$  clockwise rotation of the entire sequence after the Lower Cretaceous. This is unlikely because we find no evidence for a deformation event (angular unconformity, etc.) between the Upper Jurassic and the Lower Cretaceous. On the other hand, comparing the in situ direction of the Upper Jurassic rocks with the 50 Ma to Present poles from the Eurasian reference curve shows significant clockwise rotations ranging from  $16^\circ$  to  $23^\circ$ , on the same order as the Lower Cretaceous rocks ( Fig. 5d). Thus, the simplest interpretation is that the Upper Jurassic rocks were folded then overprinted in the Tertiary and the entire section was subsequently rotated.

We also measured the anisotropy of magnetic susceptibility of 84 Early Cretaceous red bed and 60 basalt samples with an AGICO KLY-3 Kappabridge. The basalts have a mean anisotropy degree ( $P'$ ) of 2% with six samples having  $P'$  from 5 to 14% (Fig. 6). The anisotropy shape factor ( $T$ ) varies widely, independent of  $P'$ , with a mean of  $0.1\pm 0.5$  ( $1\sigma$ ). The red beds have very small degrees of anisotropy ( $P'=0.3\pm 0.2\%$ ), with only one sample exceeding 1% (Fig. 6). Anisotropy shape is randomly distributed between prolate and oblate forms. Although the principal anisotropy directions are relatively dispersed, the mean maximum anisotropy ( $k_1$ ) directions of the basalt ( $D=318^\circ$ ,  $I=4^\circ$ ) and red beds ( $D=298^\circ$ ,  $I=-4^\circ$ ) trend roughly parallel to the strike of the fold axis defined by the bedding attitudes of the basalts ( $288^\circ\text{N}$ ) and red beds ( $299^\circ\text{N}$ ), respectively. Given the low degrees of anisotropy and the large scatter in the maximum susceptibility axis directions, neither the basalts nor the red beds have likely experienced significant strain due to compaction or tectonic stress.

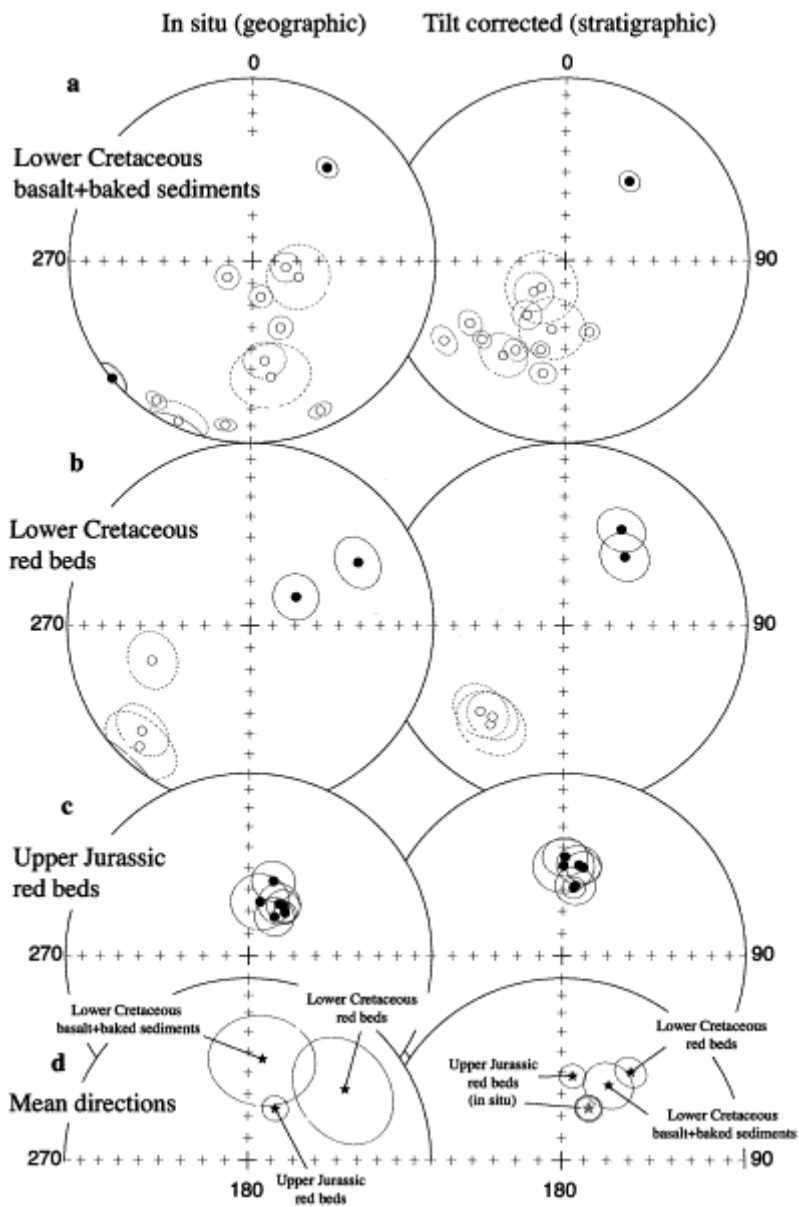


Fig. 5. Individual site mean directions in panels a–c and overall mean directions in panel d (data from Table 1).

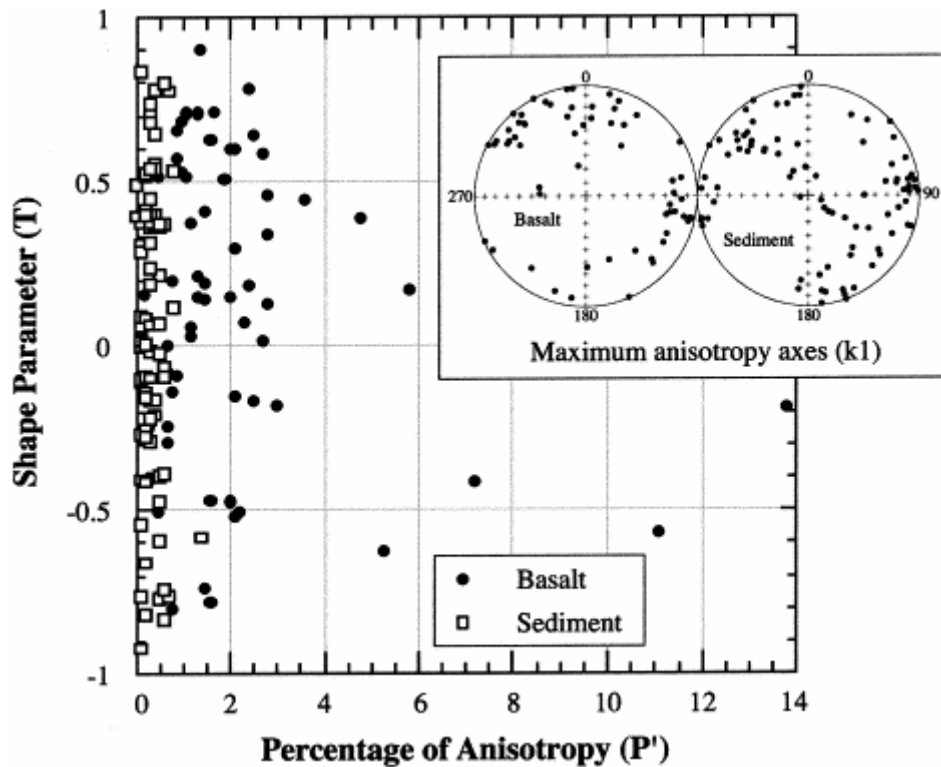


Fig. 6. Anisotropy of magnetic susceptibility data from basalts and red beds.

## 4. Discussion

From the demagnetization data and field tests we conclude that the Early Cretaceous volcanics and baked red beds, as well as five of 11 sites of Early Cretaceous red beds possess primary magnetizations. Interestingly, except for c915 which comes from the very base of the section, all the volcanic flows and two sites of baked sediments have reversed polarities. Sample 91T111, dated by Sobel and Arnaud [17], was collected in the vicinity of sites c908–c912 (E. Sobel, personal communication, 2002). They found that the weighted mean age of the whole rock sample compared well with both the total fusion and inverse isochron ages. The plagioclase fraction yielded a discordant release spectrum and the individual steps had large uncertainties due to small amounts of released  $^{39}\text{Ar}$ . They considered that the date defined by the whole rock sample ( $113.3 \pm 1.6$  Ma) best represents the age of the basalt flows, consistent with the common observation that basaltic groundmass has much higher potassium concentrations and more reliable release spectra than plagioclase. Assuming the whole rock age is correct, then the Tuoyun section helps constrain the age of the reversed polarity chron near the start of the Cretaceous Long Normal magnetic polarity superchron. However, there is some confusion in correlating the Tuoyun section with the geomagnetic polarity time scale (GPTS). According to some GPTS, sites c901–c912 correlate well in time with chron M-0 (called CM1 by Hallam et al. [25] and M-1r by Gradstein et al. [26]), near the base of the Aptian, between 113.4 and 114.0 Ma [27 and 28]. These GPTS include a younger reversed chron, sometimes referred to as ISEA, after the site of reversed polarity discovered by Vandenberg et al. [29] in the upper Aptian at  $\sim 108$  Ma (e.g., [30 and 31]). Other GPTS place M-0 at  $\sim 121$  Ma and ISEA at  $\sim 118$  Ma (see references in Berggren et al. [32]). Although this ambiguity is not resolved here, what is important is that: (1) we have clearly identified a reversed polarity interval dated at  $113 \pm 1.6$  Ma and (2) as both the M-0 and ISEA events are

thought to span about a half million years, the time represented by sites c901–c912 and c915 should be sufficient to average secular variation.

The overall mean directions of the basalt series and red bed sites are not distinct at 95% confidence limits [33] ( Fig. 5d). Although the mean inclination of the red beds ( $38.6\pm 6.8^\circ$ ) lies within statistical uncertainty of that of the basalts ( $49.9\pm 10.6^\circ$ ), the mean value remains the one with maximum probability, hence the basalts likely have steeper inclinations than the red beds. Translated into paleolatitudes, the basalts indicate a more temperate position at  $32.8\pm 9.6^\circ$  versus the red beds at  $22.0\pm 4.9^\circ$ , amounting to a difference of  $11.8\pm 10.8^\circ$ . With respect to the 110 Ma Siberian reference pole of Besse and Courtillot [24], the basalts show insignificant poleward displacement ( $3.9\pm 8.1^\circ$ ) whereas the red beds show significant poleward displacement ( $14.7\pm 4.6^\circ$ ). Thus, comparing these two results independently with the Siberian reference APWP, the interpretation would normally be that the red beds underwent significant intracontinental shortening whereas the basalts did not.

Finally we turn to the extensive central Asian paleomagnetic database of red bed sediments which was compiled by Gilder et al. [8] for 25 Early Cretaceous to Present studies demonstrating positive fold tests that lie north of the Tibetan plateau between  $34.7^\circ\text{N}$  and  $44.2^\circ\text{N}$  latitude and  $66.9^\circ\text{E}$  and  $103.5^\circ\text{E}$  longitude. The database is complemented here with 13 new poles from continental sediments meeting the same criteria ( Table 2). Although age uncertainties of continental sediments can be large, most often they are constrained at the epoch level. We also compiled all available paleomagnetic poles derived from volcanic rocks from the same region. As the database is much smaller, we accepted poles distributed over a broader area than that for the red beds, but still north of the Tibetan Plateau (Table 2 and Fig. 1). Because of the low number of studies, we accepted results obtained from a minimum of three discrete flows. We note that several poles were obtained from the Dragon database of McElhinny and Smethurst [34] where details surrounding the data are limited, especially those from Russian publications. For each pole, we calculated the paleolatitude for a common point ( $39^\circ\text{N}$ ,  $82^\circ\text{E}$  – center of Tarim Basin).

First we compared the paleolatitude data west of  $85^\circ\text{E}$  because the red bed and volcanic sites there are relatively intermingled and come from a similar tectonic setting. These data are shown in Fig. 7a compared against the paleolatitudes calculated from the Besse and Courtillot [24] Eurasian reference APWP at the same common point. Although within uncertainty limits, the mean paleolatitudes defined by the volcanic rocks are systematically  $2\text{--}4^\circ$  lower than those defined by the reference APWP. The paleolatitudes of the red beds are significantly lower by  $10\text{--}25^\circ$  than those predicted from the reference Eurasian APWP for any given age, except for two studies around 120 Ma.

Table 2. Paleomagnetic poles of Asian red beds and volcanic rocks north of the Tibetan Plateau

Slat (°N)	Slon (°E)	Age	Mean age (Ma)	Plat (°N)	Plon (°E)	Age	No.	Reference
<i>Red beds</i>								
38.6	91.1	u. Neogene	3.5	86.5	254.2	5.7	10	[39]
39.8	76.2	u. Neogene	3.5	73.9	297.5	1.9	258s	[11]
37.5	95.3	l. Pliocene	4.4	71.3	264.3	5.3	20	[40]
38.3	90.9	u. Miocene–Pliocene	8.4	79.9	274.5	3.2	19	[39]
38.2	88.7	Neogene	12.7	72.8	261.9	23.3	3	[39]
38.5	80.5	l. Neogene	14.5	58.6	210.0	6.2	30	[41]
38.7	92.8	l. Neogene	17.5	75.1	243.5	5.1	16	[40]
38.1	86.6	Paleogene–Neogene	29.6	75.8	229.5	9.6	7	[39]
39.4	93.8	Oligocene	30.2	63.9	219.7	9.8	6	[39]
38.4	94.3	Paleogene	41.0	63.4	211.2	9.9	7	[39]
37.5	86.7	Cretaceous–Paleogene	82.0	65.1	206.9	18.2	6	[39]
40.2	75.3	l. Cretaceous	115.0	53.2	183.4	6.1	5	This study
39.9	97.7	l. Cretaceous	121.0	75.5	169.9	7.7	9	[42]
<i>Basalts</i>								
50.5	105.0	Quaternary	0.5	86.0	180.0	4.6	23s	[43] – in [35]
51.0	104.0	u. Pliocene	2.5	83.0	133.0	5.0	42s	[34] – in [35]
36.3	79.0	K–Ar 12.7 and 5.8 Ma	9.3	87.7	358.8	9.7	5	[14]
52.0	101.0	Between 23 and 2 Ma	12.5	76.0	241.0	4.0	10	[34] – in [35]
46.5	96.5	Between 24 and 5 Ma	14.5	77.0	162.0	21.2	4	[44] – in [35]
41.0	114.7	K–Ar from 26 to 4 Ma	15.0	83.4	192.8	6.2	49	[45]
41.5	116.0	K–Ar from 26 to 14 Ma	20.0	88.6	29.2	8.2	13	[46]
40.7	76.1	l. Eocene ca. 54 Ma	54.0	77.0	187.5	4.4	18	[13]
42.0	75.0	K–Ar 55 to 65 Ma	60.0	76.0	190.0	4.5	3	[43] – in [35]
71.5	111.0	Cenomanian to Albian	101.0	66.0	170.0	11.0	12	[47] – in [35]
40.2	75.3	Ar–Ar 113 ± 1.6 Ma	113.0	64.1	172.1	12.0	13	This study
50.5	107.5	K–Ar 110 to 130 Ma	120.0	73.0	158.0	6.7	3	[43] – in [35]
51.2	112.2	K–Ar 118 to 128 Ma	123.0	58.5	176.8	5.6	12	[48]
51.8	117.5	Ar–Ar 125 to 133 Ma	129.0	86.8	61.8	7.4	12	[48]
41.5	72.2	Hauterivian	133.0	82.0	252.0	4.7	10	[49] – in [35]

Abbreviations: Slat (Plat), latitude of site (pole); Slon (Plon), longitude of site (pole); No., number of sites or samples (s) used to calculate mean pole; u, upper; l, lower, 25 other red bed poles given in table 3 of Gilder et al. [8].

We then took the entire set of paleomagnetic poles and calculated the corresponding paleolatitude for the same common point as before (Fig. 7b). For the red beds, we determined the average paleolatitude from 0 to 140 Ma via a sliding window with a width of nine studies moved every four studies. As the volcanic data are much fewer, we did not fit a sliding window but merely plotted each individual datum on Fig. 7b, again versus the paleolatitudes calculated from the reference APWP. Although the data are not evenly spaced in time, one notes a good correlation between the reference APWP and volcanic data, with the exception of one point with a low paleolatitude of 26°. This datum at 12.5 Ma reportedly comprises 10 sites, although the number of flows that the sites represent is unknown (Davydov et al. [35], data obtained from [34]). Given the uncertainties surrounding it, the soundest interpretation is that paleolatitudes derived from volcanic rocks show no significant deviation with respect to those calculated from the reference curve whereas the red beds are shifted toward significantly lower paleolatitudes.

Because only two volcanic studies lie within the period 20–100 Ma, comparison of volcanic and sedimentary data in that window is clearly underdetermined. We thus calculated the average difference in paleolatitude ( $\text{plat}_{\text{volc}} - \text{plat}_{\text{sed}}$ ) in two time windows: 0–20 Ma and 110–133 Ma, which is  $15.5 \pm 6.6^\circ$  and  $9.9 \pm 9.6^\circ$ , respectively. These results again indicate that Cretaceous to Present red beds in central Asia have systematically lower paleolatitudes than coeval volcanics. However, the discrepancy is less for the Early Cretaceous than for the Neogene, and the variance decreases toward the present, both of which may suggest that the process leading to shallow inclinations has changed with time.

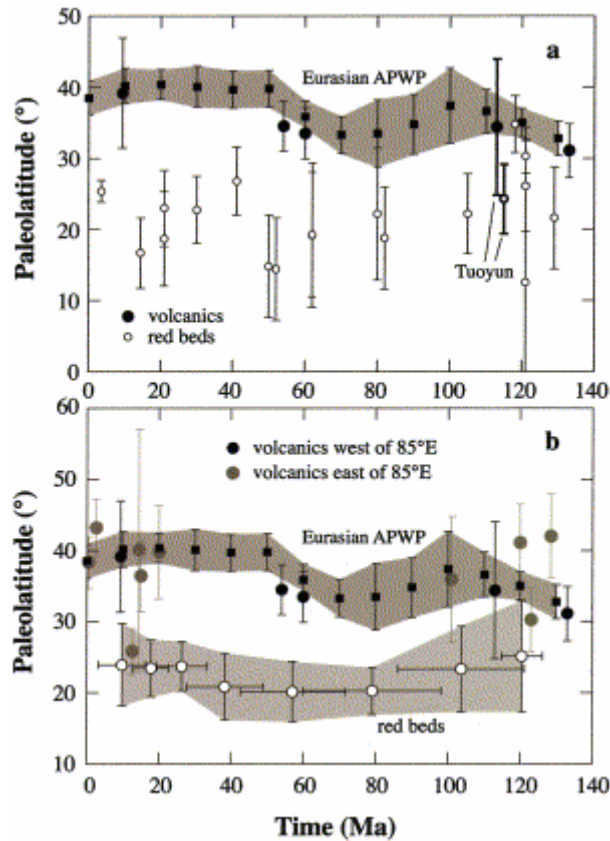


Fig. 7. Paleolatitudes calculated from poles listed in Table 2 and Gilder et al. ( [8], table 3) for a common site at 39°N, 82°E (center of Tarim Basin) for red beds, volcanic rocks and from the reference Eurasian APWP from Besse and Courtillot [24]. (a) From localities lying west of 85°E (see Fig. 1). (b) For all data in Table 2 and Gilder et al. ( [8], table 3). Red beds are treated using a sliding window of nine studies moved every four studies (last step is 11 studies).

To explain the central Asian shallow inclinations, Tan et al. [10] conducted a paleomagnetic and magnetic fabric study of Cretaceous red beds from the Tarim Basin and concluded that shallowing occurs during deposition and compaction. A similar study of the Subei section in the Qaidam basin suggested that shallowing was produced partly by imbrication during sedimentation under northward-directed transport conditions [8]. To explain how the Subei study could apply to the whole of central Asia, we recall that rivers eroding the east–west-trending mountain ranges of central Asia flow on average to the north, because the deformation front propagates northward as India penetrates Asia from the south [36]. Because mountain building in central Asia has probably intensified since the Cretaceous, this could partially explain why the shallowing effect has amplified from the Cretaceous to Present. Numerical experiments show that faster sedimentation rates can produce more inclination shallowing than slower rates [37], and given that sedimentation rate in central Asia has increased from the Cretaceous to Present [38], the shallowing problem can be exacerbated with time. This leads to the possibility that systematic differences in deposition transport direction, rate and/or energy can explain why some red beds show no (or little) evidence for shallowing, whereas others do. For example, Cretaceous paleolatitudes of red beds from the North and South China blocks are not lower than expected – in most cases these red beds were deposited in low energy environments, in north–south-trending basins formed during east–west extension; thus, sedimentation conditions in the Cretaceous in central Asia were likely much different than in North and South China. Finally, we note that, because the Cretaceous and the Cenozoic paleolatitudes predicted from the synthetic APWP are not much

different ( $\sim 5^\circ$ ) ( Fig. 7), flattening effects due to compaction should not be different from one time to another, as amounts of compaction-induced inclination shallowing are latitude-dependent. One potential difference could be that the magnetic remanences of Cretaceous rocks are chemical in origin whereas those of Neogene rocks are detrital. Unfortunately, no data exist to test this hypothesis.

The conclusion from our work is that the paleolatitudes of 140 Ma to Present volcanic rocks coincide well with coeval paleolatitudes predicted from the synthetic reference APWP. This suggests: (1) that the reference curve is likely representative of stable Eurasia, and (2) that no long-standing non-dipole field anomaly existed in the region. This was the conclusion of Bazhenov and Mikolaichuk [13] for their Paleocene result which we show to be true for the Cretaceous and the entire Cenozoic. Finally, it should be clear that the Neogene red beds in the part of central Asia considered here systematically underdetermine ( $15.5 \pm 6.6^\circ$ ) predicted inclinations (paleolatitudes). This is also seen in Cretaceous red beds, however, the effect is smaller ( $9.9 \pm 9.6^\circ$ ). We conclude that one cannot fully trust paleogeographic reconstructions based on red bed studies alone, especially during periods of high sedimentation rate/energy. On the positive side, we find that volcanic data do provide correct estimates and that non-dipole field models are not required, or even supported by the data.

## Acknowledgements

We thank R. Enkin for helpful comments. IPGP contribution #1861

## References

1. Y. Chen, V. Courtillot, J.P. Cogné, J. Besse, Z.Y. Yang and R. Enkin, The configuration of Asia prior to the collision of India: Cretaceous paleomagnetic constraints. *J. Geophys. Res.* **98** (1993), pp. 21,927–21,941.
2. J.C. Thomas, H. Perroud, P.R. Cobbold, M.L. Bazhenov, V.S. Burtman, A. Chauvin and E. Sadybakasov, A paleomagnetic study of Tertiary formations from the Kyrgyz Tien-Shan and its tectonic implications. *J. Geophys. Res.* **98** (1993), pp. 9571–9589.
3. J.C. Thomas, A. Chauvin, D. Gapais, M.L. Bazhenov, H. Perroud, P.R. Cobbold and V.S. Burtman, Paleomagnetic evidence for Cenozoic block rotations in the Tadjik depression (central Asia). *J. Geophys. Res.* **99** (1994), pp. 15141–15160.
4. M. Westphal, Did a large departure from the geocentric axial dipole hypothesis occur during the Eocene? Evidence from the magnetic polar wander path of Eurasia. *Earth Planet. Sci. Lett.* **117** (1993), pp. 15–28.
5. J.P. Cogné, N. Halim, Y. Chen and V. Courtillot, Resolving the problem of shallow magnetizations of Tertiary age in Asia: insights from paleomagnetic data from the Qiangtang, Kunlun, and Qaidam blocks (Tibet, China), and a new hypothesis. *J. Geophys. Res.* **104** (1999), pp. 17,715–17,734.
6. A. Chauvin, H. Perroud and M.L. Bazhenov, Anomalous low paleomagnetic inclinations from Oligocene–Lower Miocene red beds of the south-west Tien Shan, Central Asia. *Geophys. J. Int.* **126** (1996), pp. 303–313.

7. S.A. Gilder, X.X. Zhao, R.S. Coe, Z.F. Meng, V. Courtillot and J. Besse, Paleomagnetism, tectonics and geology of the southern Tarim basin, northwestern China. *J. Geophys. Res.* **101** (1996), pp. 22015–22031.
8. S. Gilder, Y. Chen and S. Sen, Oligo–Miocene magnetostratigraphy and rock magnetism of the Xishuigou section, Subei (Gansu Province, western China), and implications for shallow inclinations in central Asia. *J. Geophys. Res.* **106** (2001), pp. 30,505–30,521.
9. N. Halim, J.P. Cogné, Y. Chen, R. Atasei, J. Besse, V. Courtillot, S. Gilder, J. Marcoux and R.L. Zhao, New Cretaceous and Early Tertiary paleomagnetic results from Xining-Lanzhou basin, Kunlun and Qiangtang blocks, China: Implications on the geodynamic evolution of Asia. *J. Geophys. Res.* **103** (1998), pp. 21,025–21,045.
10. X. Tan, K.P. Kodama, H. Chen, D. Fang, D. Sun, Y. Li, Paleomagnetism and magnetic anisotropy of Cretaceous red beds from the Tarim basin, northwest China: Evidence for a rock magnetic cause of anomalously shallow paleomagnetic inclinations from central Asia, *J. Geophys. Res.* (2002).
11. J. Chen, D.W. Burbank, K.M. Scharer, E. Sobel, J.H. Yin, C. Rubin and R.B. Zhao, Magnetochronology of the Upper Cenozoic strata in the Southwestern Chinese Tian Shan: rates of Pleistocene folding and thrusting. *Earth Planet. Sci. Lett.* **195** (2002), pp. 113–130.
12. Y. Otofujii, T. Itaya, H.C. Wang and S. Nohda, Palaeomagnetism and K–Ar dating of Pleistocene volcanic rocks along the Altyn Tagh Fault, northern border of Tibet. *Geophys. J. Int.* **120** (1995), pp. 367–374.
13. M.L. Bazhenov and A.V. Mikolaichuk, Paleomagnetism of Paleogene basalts from the Tien Shan, Kyrgyzstan: rigid Eurasia and dipole geomagnetic field. *Earth Planet. Sci. Lett.* **195** (2002), pp. 155–166.
14. Y.A. Li, Q. Li, H. Zhang, D.J. Sun, Y.D. Cao and S.Z. Wu, Paleomagnetic study of Tarim and its adjacent area as well as the formation and evolution of the basin. *Xinjiang Geol.* **13** (1995), pp. 293–376.
15. Z.F. Meng, Y.S. Deng, T.H. Ding, C.P. Guang, Y.A. Li and D.J. Sun, Mesozoic–Cenozoic paleomagnetic results of volcanic rocks from the southern Tarim Basin. *Sci. China (Ser. D)* **28** (1998), pp. 79–89.
16. Chinese Bureau of Geology, Stratigraphic Tables for Xinjiang Autonomous Region, 1981, 496 pp.
17. E.R. Sobel and N. Arnaud, Cretaceous–Paleogene basaltic rocks of the Tuyon basin, NW China and the Kyrgyz Tian Shan: the trace of a small plume. *Lithos* **50** (2000), pp. 191–215.
18. J.L. Kirschvink, The least-square line and plane and the analysis of paleomagnetic data. *Geophys. J. R. Astron. Soc.* **62** (1980), pp. 699–712.
19. R.A. Fisher, Dispersion on a sphere. *Proc. R. Soc. London A* **217** (1953), pp. 295–305. MathSciNet

20. G.S. Watson and R.J. Enkin, The fold test in paleomagnetism as a parameter estimation problem. *Geophys. Res. Lett.* **20** (1993), pp. 2135–2137.
21. J.P. Cogné, PaleoMac: a Macintosh™ application for treating paleomagnetic data and making plate reconstructions, *Geochem. Geophys. Geosyst.* (2002)
22. R. Day, M. Fuller and V.A. Schmidt, Hysteresis properties of titanomagnetites: Grain size and composition dependence. *Phys. Earth Planet. Inter.* **13** (1977), pp. 260–267.
23. N.D. Opdyke, J.E.T. Channell, *Magnetic Stratigraphy*, Academic Press, San Diego, CA, 1996, 346 pp.
24. J. Besse, V. Courtillot, Apparent and true polar wander and geometry of the geomagnetic field over the last 200 Myr, *J. Geophys. Res.* 107 (B11) (2002) doi: 10.1029/2000JB000050.
25. A. Hallam, J.M. Hancock, J.L. La Brecque, W. Lowrie and J.E.T. Channell, Jurassic to Paleogene; Part 1, Jurassic and Cretaceous geochronology and Jurassic to Paleogene magnetostratigraphy. *Geol. Soc. London* **10** (1985), pp. 118–140.
26. F.M. Gradstein, F.P. Agterberg, J.G. Ogg, J. Hardenbol, P. van Veen, J. Thierry and Z.H. Huang, A Mesozoic time scale. *J. Geophys. Res.* **99** (1994), pp. 24,051–24,074.
27. J.E.T. Channell, W. Lowrie and F. Medizza, Middle and Early Cretaceous magnetic stratigraphy from the Cismon section, northern Italy. *Earth Planet. Sci. Lett.* **42** (1979), pp. 153–166.
28. W. Lowrie and J.G. Ogg, A magnetic polarity time scale for the Early Cretaceous and Late Jurassic. *Earth Planet. Sci. Lett.* **76** (1986), pp. 341–349.
29. J. Vandenberg, C.T. Klootwijk and A.A.H. Wonders, Late Mesozoic and Cenozoic movements of the Italian Peninsula; further paleomagnetic data from the Umbrian Sequence. *Geol. Soc. Am. Bull.* **89** (1978), pp. 133–150.
30. W. Lowrie, W. Alvarez, I. Premoli-Silva and S. Monechi, Lower Cretaceous magnetic stratigraphy in Umbrian pelagic carbonate rocks. *Geophys. J. R. Astron. Soc.* **60** (1980), pp. 263–281.
31. J.A. Tarduno, Brief reversed polarity interval during the Cretaceous normal polarity superchron. *Geology* **18** (1990), pp. 683–686.
32. W.A. Berggren, D.V. Kent, M.P. Aubry, J. Hardenbol, *Time Scales and Global Stratigraphic Correlation*, SEPM Spec. Publ. No. 54, 1995.
33. P.L. McFadden and F.J. Lowes, The discrimination of mean directions drawn from Fisher distributions. *Geophys. J. R. Astron. Soc.* **67** (1981), pp. 19–33.
34. M.W. McElhinny and M.A. Smethurst, The global paleomagnetic database: current status. *EOS* **82** (2001), p. 436.

35. V.F. Davydov, A.Y. Kravchinsky, Paleomagnetic directions and pole positions: Data for the USSR – Issue 1, Soviet Geophysical Committee, World Data Center-B, Moscow, Catalogue, 1971.
36. P. Tapponnier, Z.Q. Xu, F. Roger, B. Meyer, N. Arnaud, G. Wittlinger and J.S. Yang, Oblique stepwise rise and growth of the Tibet plateau. *Science* **294** (2001), pp. 1671–1677.
37. J. Jezek, S. Gilder, Competition of magnetic and hydrodynamic forces on ellipsoidal particles under shear: potential influence on the recording process of the Earth's magnetic field in sediments, EGS Abstract volume, 2002.
38. F. Métivier and Y. Gaudemer, Mass transfer between eastern Tien Shan and adjacent basins (central Asia): constraints on regional tectonics and topography. *Geophys. J. Int.* **128** (1997), pp. 1–17.
39. Y. Chen, S. Gilder, N. Halim, J.-P. Cogné and V. Courtillot, New paleomagnetic constraints on central Asian kinematics: Displacement along the Altyn Tagh fault and rotation of the Qaidam Basin. *Tectonics* **21** (2002), p. 1042.
40. G. Dupont-Nivet, R.F. Butler, A. Yin and X.H. Chen, Paleomagnetism indicates no Neogene rotation of the Qaidam Basin in northern Tibet during Indo-Asian collision. *Geology* **30** (2002), pp. 263–266.
41. G. Dupont-Nivet, Z. Guo, R.F. Butler and C. Jia, Discordant paleomagnetic direction in Miocene rocks from the central Tarim Basin: Evidence for local deformation and inclination shallowing. *Earth Planet. Sci. Lett.* **199** (2002), pp. 473–482.
42. Y. Chen, H.N. Wu, V. Courtillot and S. Gilder, Large NS convergence at the northern edge of the Tibetan plateau? New Early Cretaceous paleomagnetic data from Hexi Corridor, NW China. *Earth Planet. Sci. Lett.* **202** (2002), pp. 293–307.
43. M.I. Rozinov, L.E. Sholpo, Paleomagnetic directions and pole positions: Data for the USSR – Issue 1, Soviet Geophysical Committee, World Data Center-B, Moscow, Catalogue, 1971.
44. E.S. Gorshkov, E.G. Gooskova, V.A. Starunov, T.S. Tyuleneva, Z. Ganhuyach, P. Khosbayar, Paleomagnitnie issledovaniya v zentralnoy Mongolii, in: IV All-Union Congress on Geomagnetism, Vladimir-Suzdal, vol. 2 (1991) 116–117.
45. Z. Zheng, M. Kono, H. Tsunakawa, G. Kimura, Q. Wei, X. Zhu and T. Hao, The apparent polar wander path for the North China Block since the Jurassic. *Geophys. J. Int.* **104** (1991), pp. 29–40.
46. X. Zhao, R.S. Coe, Y. Zhou, H. Wu and J. Wang, New paleomagnetic results from northern China collision and suturing with Siberia and Kazakhstan. *Tectonophysics* **181** (1990), pp. 43–81.
47. B.V. Gusev, Paleomagnetic directions and pole positions: Data for the USSR – Issue 2, Soviet Geophysical Committee, World Data Center-B, Moscow, Catalogue, 1973.

48. N. Halim, J.P. Cogné, V.A. Kravchinsky, New Mesozoic paleomagnetic results from the Mongol-Okhotsk suture zone: clues on the late Jurassic oceanic closure and the post-Cretaceous left-lateral shear of the Trans-Baikal area (Siberia), *J. Geophys. Res.* (2001)

49. K.A. Abdullaev et al., Paleomagnetic directions and paleomagnetic pole positions: Data for the former USSR – Issue 8, VNIGRI Institute, St. Petersburg (unpublished), Catalogue, 1993.